XRD, Electron Microscopy and Vibrational Spectroscopy Characterization of Simulated High-Fe/Al HLW Glasses – 15666

Sergey Stefanovsky *, Boris Nikonov **, James Marra ***
* Frumkin Institute of Physical Chemistry and Electrochemistry RAS
** Institute of Geology of Ore Deposits RAS
*** Savannah River National Laboratory

ABSTRACT

Sample glasses have been made using SB6 high level waste (HLW) simulant (high in both Al and Fe) with 12 different frit compositions at a constant waste loading of 36 wt.%. As follows from X-ray diffraction (XRD) and optical and scanning electron microscopy (SEM) data, all the samples are composed of primarily glass and minor concentration of spinel phases which form both isometric grains and fine cubic (~1 μm) crystals. Infrared (IR) spectra of all the glasses within the range of 400-1600 cm^{-1} consist of the bands due to stretching and bending modes in silicon-oxygen, boron-oxygen, aluminum-oxygen and iron-oxygen structural groups. Raman spectra showed that for the spectra of all the glasses within the range of 850-1200 cm^{-1} the best fit is achieved by suggestion of overlapping of three major components with maxima at 911-936 cm^{-1}, 988-996 cm^{-1} and 1020-1045 cm^{-1}. The structural network is primarily composed of metasilicate chains and possibly rings with embedded AlO_4 and FeO_4 tetrahedra. Major BO_4 tetrahedra and BO_3 triangles form complex borate units and are present as separate constituents.

INTRODUCTION

Ferrous compounds frequently occur in nuclear waste as both activated corrosion products and process chemicals. Some waste streams such as liquid high level waste (HLW) stored in tanks at the Savannah River Site (SRS) may contain up to nearly 30 wt.% Fe_2O_3 [1,2]. Incorporation of iron oxides into glass has multiple effects on the structure and properties of borosilicate glasses. Boron in boron-containing glasses may be present in trigonal and tetrahedral coordination. Borosilicate glasses containing major tetrahedrally coordinated boron have higher chemical durability than those with predominantly trigonally coordinated boron [3]. This is especially important for nuclear waste glasses because chemical durability is a key factor determining their suitability for long-term immobilization of radionuclides.

The relative ratio between three and four coordinated boron is estimated from the structural factors ψ_B, which is the molar ratio of the sum of oxides capable to deliver oxygen to convert BO_3 triangles to BO_4 tetrahedra, to B_2O_3 concentration in the glass and can be calculated as suggested in ref. [3]

$$\psi_B = \{(Na_2O+K_2O+BaO)+[0.7(CaO+SrO+CdO+PbO)+[0.3(Li_2O+MgO+ZnO)]-Al_2O_3\}/B_2O_3 \quad (1),$$

and K calculated as a ratio of molar concentrations

$$K = [SiO_2] / [B_2O_3] \quad (2)$$

The higher ψ_B and K values, the higher fraction of four-coordinated boron in the glass structure. Tetrahedral environment is known to be stable at [4]

$$0.225 \leq r_i/r_O \leq 0.414, \quad (3)$$

where r_i and r_O are the radii of tetrahedrally coordinated cation and O^{2-} anion, Å.

The r_i values for B^{3+}, Al^{3+}, and Fe^{3+} ions are 0.11, 0.39, and 0.49 Å, respectively [5]. For radius of O^{2-} anion r_O = 1.38 Å the r_i/r_O values for same cations are 0.080, 0.283, and 0.355, respectively. Thus oxygen is preferentially spent to form AlO_4 and FeO_4 tetrahedra rather than BO_4 tetrahedra.

The partitioning of boron between trigonal and tetrahedral coordinations in aluminoborosilicate glass systems can be determined quantitatively using the nuclear magnetic resonance (NMR) technique [6-11]. However, the presence of iron as well as other paramagnetic species in glasses prevents the use of NMR due to significant broadening of the spectral lines [12,13]. The objective of this work is to apply the insight gained from studying the impact of varying levels of boron, alkali, and some additives such as Ca and Mn on the coordination chemistry of simulated HLW glass systems using different methods such as IR and Raman spectroscopy.

METHODS

Sample glasses have been made at SRNL using SB6 simulant (high in both Al and Fe – Table I) with 12 different frit compositions at a constant waste loading of 36 wt.% (Table II). The baseline frit composition was Frit 418 and the remaining frit compositions contained 8 to 16 wt% B_2O_3, 4 to 8 wt% Na_2O, 0 to 4 wt% MnO and 0 to 2 wt% CaO.

Table I. Chemical Composition of SB6-CEF Surrogate.

Elements	wt.%	Oxides	wt.%
Fe	18.90	Fe_2O_3	27.02
Al	15.90	Al_2O_3	29.05
Mn	5.92	MnO	7.64
Ca	0.95	CaO	1.33
Mg	0.45	MgO	0.75
Ni	2.54	NiO	3.23
Cu	0.18	CuO	0.23
Ti	0.01	TiO_2	0.02
Si	0.14	SiO_2	0.30
Na	15.40	Na_2O	20.76
K	0.07	K_2O	0.08
Sr	0.05	SrO	0.06
Zr	0.21	ZrO_2	0.29
S	0.37	SO_3	0.92
Total	61.09	Total	91.68

The ψ_B values range between 0.79 and 2.14 at moderate silica contents (50-54 mol.%). These values point to a significant fraction of trigonally coordinated boron. The glasses #35 and #40 should have the highest fraction of tetrahedrally coordinated boron, whereas the glass #46 – the lowest one.

Each of the glasses was prepared from waste surrogate and frit in 50 mL Pt crucible. The crucibles were placed into a resistive furnace, heated to a temperature of 1150 °C, kept at this temperature for 1 hr, and removed from the furnace. Melts were poured onto a stainless steel plate, and cooled in air.

Powdered samples were examined by XRD using a Rigaku D / Max 2200 diffractometer (Cu Kα radiation). Polished samples were studied by optical microscopy using an OLYMPUS BX51 polarizing microscope. SEM examination was performed using a JSM 5610 LV + JED-2300 analytical unit (metals, oxides, phosphates and silicates were used as standard). IR spectra were recorded at a modernized IKS-29 spectrophotometer (compaction of powdered glasses in pellets with KBr) within the range of 4000–400 cm^{-1}. Raman spectra were recorded using a Jobin Yvon U1000 spectrophotometer operated at an excitation wavelength of 532 nm.

Table II. Glass compositions.

Oxides	35		36		37		38		39		40		41		42		43		44		45		46	
	wt.%	mol. %	wt.%	mol. %	wt.%	mol. %	wt.%	mol. %	wt.%	mol. %	wt.%	mol. %	wt.%	mol. %	wt.%	mol. %	wt.%	mol. %	wt.%	mol. %	wt.%	mol. %	wt.%	mol. %
Li_2O	5.12	11.41	5.12	11.47	5.12	11.44	5.12	11.46	5.76	12.83	5.12	11.42	5.12	11.43	5.12	11.45	5.12	11.41	5.12	11.42	5.12	11.44	5.12	11.49
B_2O_3	5.12	4.90	8.96	8.62	7.04	6.75	7.04	6.76	7.04	6.73	5.12	4.90	5.12	4.91	5.12	4.91	5.12	4.89	5.12	4.90	5.12	4.91	10.24	9.86
Na_2O	12.59	13.52	12.59	13.60	12.59	13.56	11.31	12.20	10.67	11.45	12.59	13.54	11.95	12.86	11.31	12.20	11.95	12.83	11.31	12.16	11.31	12.18	10.03	10.85
MgO	0.27	0.45	0.27	0.45	0.27	0.45	0.27	0.45	0.27	0.45	0.27	0.45	0.27	0.45	0.27	0.45	0.27	0.45	0.27	0.45	0.27	0.45	0.27	0.45
Al_2O_3	10.78	7.04	10.78	7.08	10.78	7.06	10.78	7.07	10.78	7.03	10.78	7.05	10.78	7.05	10.78	7.07	10.78	7.04	10.78	7.04	10.78	7.06	10.78	7.09
SiO_2	48.75	54.01	44.91	50.05	46.83	52.03	46.83	52.12	45.55	50.43	48.11	53.36	48.11	53.40	47.47	52.80	47.47	52.58	47.47	52.63	46.19	51.32	46.19	51.53
SO_3	0.33	0.27	0.33	0.28	0.33	0.28	0.33	0.28	0.33	0.27	0.33	0.27	0.33	0.27	0.33	0.28	0.33	0.27	0.33	0.27	0.33	0.28	0.33	0.28
K_2O	0.03	0.02	0.03	0.02	0.03	0.02	0.03	0.02	0.03	0.02	0.03	0.02	0.03	0.02	0.03	0.02	0.03	0.02	0.03	0.02	0.03	0.02	0.03	0.02
CaO	0.48	0.57	0.48	0.57	0.48	0.57	0.48	0.57	0.48	0.57	0.48	0.57	0.48	0.57	0.48	0.57	1.76	2.09	1.76	2.09	1.76	2.10	0.48	0.57
TiO_2	0.01	0.01	0.01	0.01	0.01	0.01	0.01	0.01	0.01	0.01	0.01	0.01	0.01	0.01	0.01	0.01	0.01	0.01	0.01	0.01	0.01	0.01	0.01	0.01
MnO	2.75	2.58	2.75	2.60	2.75	2.59	4.03	3.80	5.31	4.98	3.39	3.18	4.03	3.79	5.31	5.00	3.39	3.18	4.03	3.78	5.31	5.00	2.75	2.60
Fe_2O_3	9.73	4.06	9.73	4.08	9.73	4.07	9.73	4.07	9.73	4.05	9.73	4.06	9.73	4.06	9.73	4.07	9.73	4.06	9.73	4.06	9.73	4.07	9.73	4.08
NiO	1.16	1.03	1.16	1.04	1.16	1.04	1.16	1.04	1.16	1.03	1.16	1.04	1.16	1.04	1.16	1.04	1.16	1.03	1.16	1.03	1.16	1.04	1.16	1.04
CuO	0.08	0.07	0.08	0.07	0.08	0.07	0.08	0.07	0.08	0.07	0.08	0.07	0.08	0.07	0.08	0.07	0.08	0.07	0.08	0.07	0.08	0.07	0.08	0.07
SrO	0.02	0.01	0.02	0.01	0.02	0.01	0.02	0.01	0.02	0.01	0.02	0.01	0.02	0.01	0.02	0.01	0.02	0.01	0.02	0.01	0.02	0.01	0.02	0.01
ZrO_2	0.11	0.06	0.11	0.06	0.11	0.06	0.11	0.06	0.11	0.06	0.11	0.06	0.11	0.06	0.11	0.06	0.11	0.06	0.11	0.06	0.11	0.06	0.11	0.06
Sum	97.33	100.0	97.33	100.0	97.33	100.0	97.33	100.0	97.33	100.0	97.33	100.0	97.22	100.0	97.33	100.0	97.33	100.0	97.33	100.0	97.33	100.0	97.33	100.0
ψ_B		2,14		1.22		1.56		1.35		1.25		2.14		2.00		1.86		2.00		1.86		1.86		0.79
ψ_B(Fe)*		1.89		1.08		1.37		1.17		1.07		1.89		1.75		1.61		1.75		1.61		1.61		0.66
K		11.0		5.8		7.7		7.7		7.5		10.9		10.9		10.8		10.8		10.7		10.5		5.2

* $\psi_B(Fe) = \{(Na_2O+K_2O+BaO)+[0.7(CaO+SrO+CdO+PbO)+[0.3(Li_2O+ MgO+ZnO)]-Al_2O_3-0.3Fe_2O_3\} / B_2O_3$ [3]

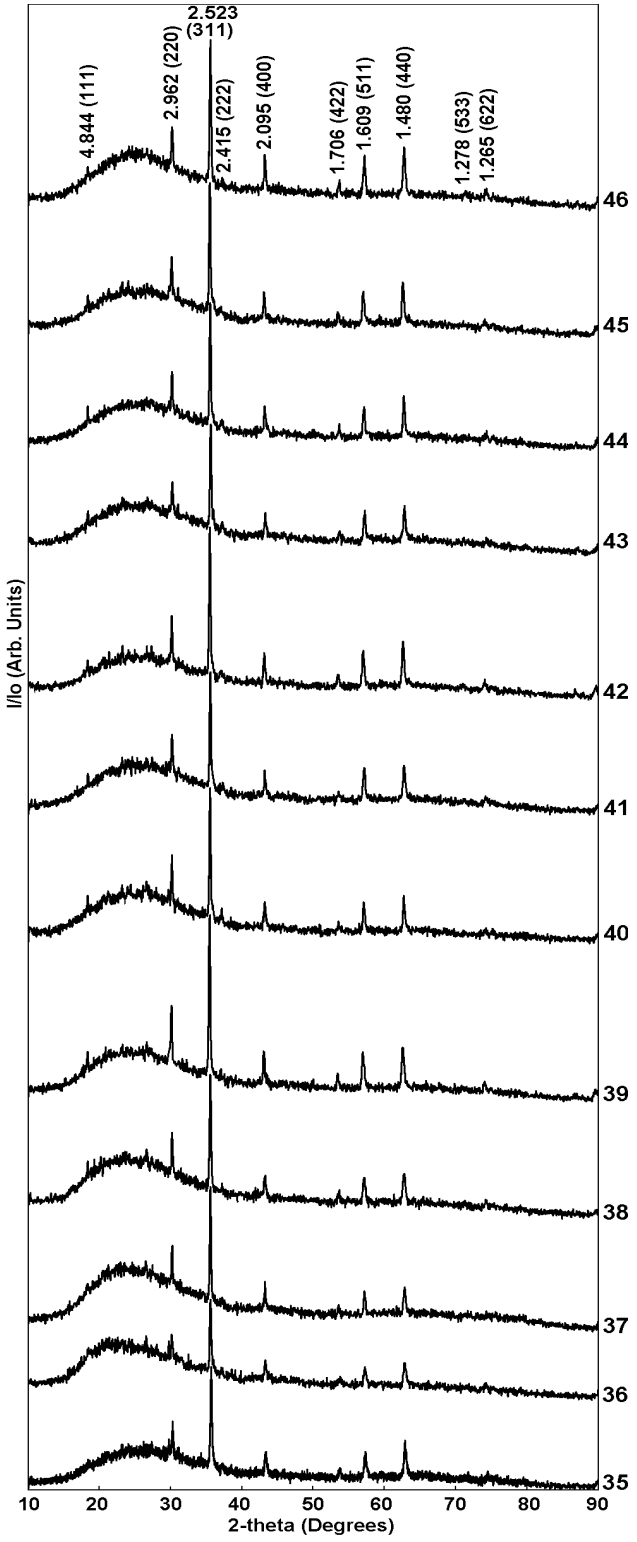

Figure 1. XRD patterns of the samples.

All the reflections are due to spinel.

RESULTS AND DISCUSSION

XRD study

XRD patterns show that all the samples are composed of a major vitreous phase and a minor spinel structure phase (Figure 1). Spinel is normally formed in borosilicate nuclear waste glasses containing iron and other transition metal oxides (Cr_2O_3, MnO, Mn_2O_3, CoO, NiO, CuO) [14,15]. Because the lattice parameter of the spinel phase is nearly same in all the samples, it may be suggested that the chemical composition of this phase is also similar in all the samples.

Optical and Electron Microscopy Study

A photomicrograph of sample #35 (Figure 2*a*) shows the dominance of light transparent glass containing spinel crystals as both isometric grains tens of microns in size and the fine crystals of about 1 μm in size. The glass matrix contains wavy bands displaying features of flowing melt and differing in amount of fine crystals in glass. Wavy-banded distribution of fine crystals causes fluidal texture of the glass, which is typical for glassy volcanic rocks. Moreover, gas bubbles from tens to hundreds microns in diameter are evident. A detail of the sample seen in Figure 2*a* at higher magnification demonstrates that the spinel phase forms fine cubic crystals about 1 μm in size (Figure 2*b*). This photomicrograph clearly identifies features of distribution of fine crystals in the glass.

A specific feature of the glassy matrix in sample #36 is a light-brown colored glass and relatively low content of spinel crystals within the glass (Figure 2*c*). Spinel forms either irregular grains or elongated wavy-type grains emphasizing elements of the fluidal texture. Minor fine cubic crystals of spinel are also present. Gas bubbles 50-200 μm in diameter occur in the vitreous phase and are non-uniformly distributed.

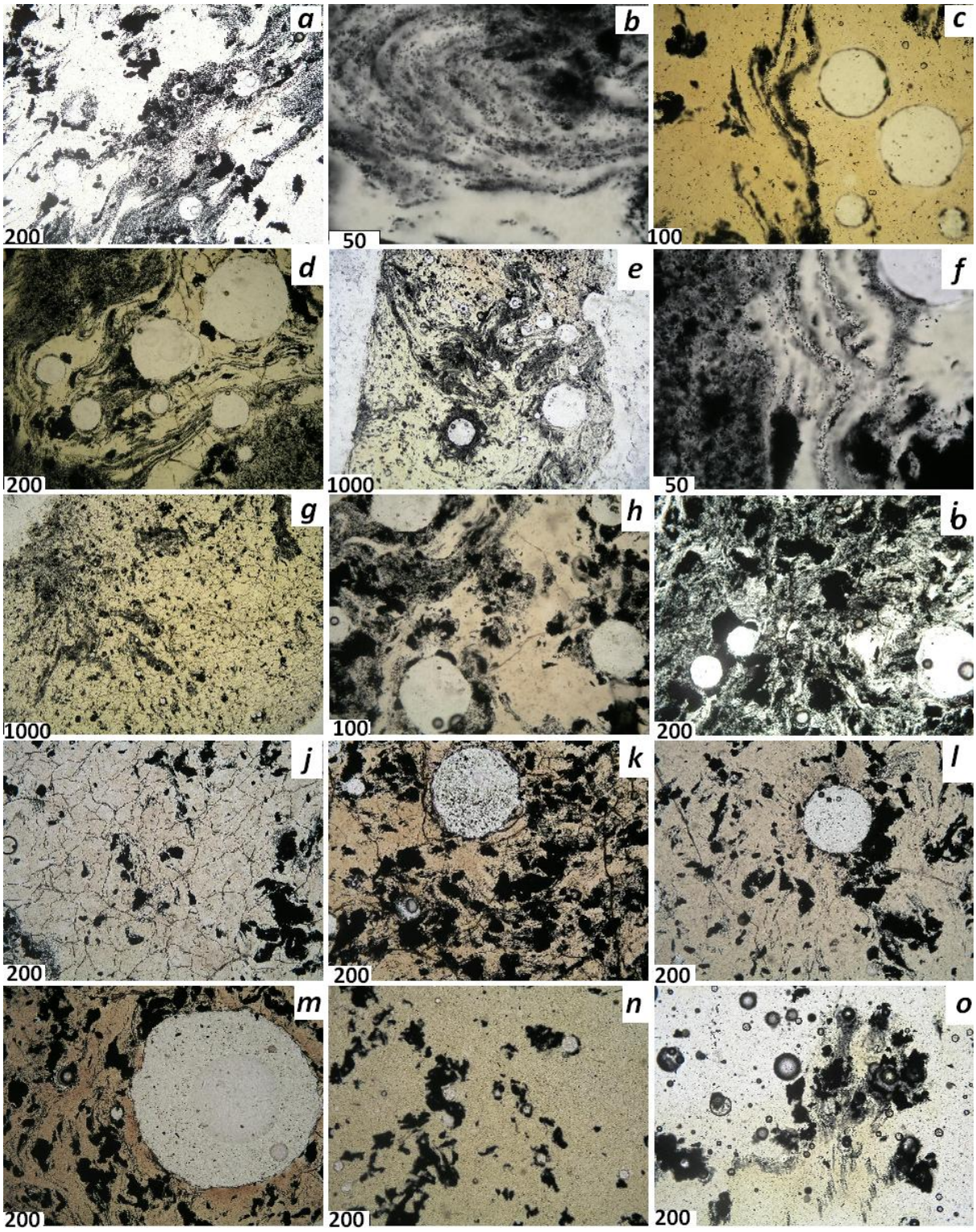

Figure 2. Optical microscopy images of the samples.

Scale bars are given in microns.

Figure 2*d* illustrates a general view of sample #37. The glassy matrix is characterized by a clearly defined fluidal texture and light-brown coloring. Spinel crystals are rather non-uniformly distributed over the bulk and occur predominantly as fine (~1 μm in size) crystals. The glassy phase contains numerous gas bubbles up to 0.5 mm in diameter.

Figure 2*e* demonstrates a fragment of the same sample enriched with spinel. It is readily apparent that fluidity is represented by alternating wavy bands enriched and depleted with fine cubic spinel crystals. Dense aggregates of cubic spinel crystals are occasionally observed. As seen at higher magnification (Figure 2*f*), spinel occurs as both individual cubic crystals about 1 μm in size and aggregates of fine crystals forming dense opaque areas.

Glass in the thin section of sample #38 has light-brown coloring and is characterized by cracking illustrating high mechanical stress (Figure 2*g*). The amount of spinel phase is rather minor with the spinel present primarily as isometric grains. Fine cubic crystals are concentrated in a small area of the sample. Wavy-banded distribution of fine cubic crystals defines the fluidal texture of this area.

The thin section of sample #39 shows a light-brown glass with high concentrations of spinel and gas bubbles (Figure 2*h*). Spinel is present as both isometric grains and fine cubic crystals. There are areas both enriched with fine crystals and free of crystals. One area displays clear fluidal texture. Cracking is negligible.

The glassy matrix in the thin section of sample #40 is strongly enriched with spinel (Figure 2*i*). Spinel occurs as both isometric grains and fine cubic crystals. Fluidity is apparent locally. Areas not containing spinel are small in size and occur rarely. In spite of the high spinel content, the glassy phase is light and transparent. Microcracking of the glass is negligible.

The glassy matrix in the thin section of sample #41 (Figure 2*j*) has low spinel content (<10 vol.%). Nearly all the spinel forms isometric grains. The amount of fine crystals is negligible. The glassy phase has light brown-green coloring and cracks due to mechanical stresses.

The thin section of sample #42 is represented by glass with high concentrations of spinel and gas bubbles (Figure 2*k*). Bubbles are up to 200 μm in size. Glass has brown color and fluidity is poorly defined. Spinel crystals form predominantly isomeric grains. The concentration of fine cubic crystals is negligible.

The thin section of sample #43 is composed of light colored brown-green glass with minor spinel crystals forming isometric grains (Figure 2*l*). Spinel content may be estimated as 6-8 vol.%. The microstructure contains minor concentrations of aggregates of fine crystals and gas bubbles up to 200 μm in diameter. Cracking is negligible.

The microstructure of sample #44 is composed of green-brown glass with high spinel content (25-30 vol.%). The majority of spinel is represented by isometric randomly distributed grains. Minor fine cubic crystals identify the fluidal texture of the glassy matrix due to their wavy-banded distribution over the matrix. Large (up to 1.5 mm in diameter) gas bubbles are also present. Microcracking is nearly absent (Figure 2*m*).

The thin section of sample #45 is composed of yellow-green glass with minor spinel content (~10 vol.%) – see Figure 2*n*. The majority of spinel is present as isometric grains. Fine cubic crystals with a wavy-banded distribution are present in local areas. Individual gas bubbles 10-20 μm in diameter are also present. In crossed Nichols polarization, areas with weakly defined double reflection (probably due to initial stage of glass devitrification) were found.

The microstructure of sample #46 (Figure 2*o*) is composed of non-uniformly colored (from clear transparent to light-yellow) glass with minor spinel crystal concentration (5-10 vol.%). The majority of

spinel is present as randomly distributed isometric grains. A minor concentration of spinel present as fine cubic crystals occurred in localized areas. The latter forms short discontinuous bands. The glass contains numerous small gas bubbles generally <20 μm in diameter.

The SEM study confirmed XRD and optical microscopy data. All the samples contain two spinel varieties (Figure 3). The primary spinel occurs as individual cubic crystals up to ~50 μm in size (Figure 3, left). The secondary spinel is present as aggregates of fine (1-10 μm) crystals (dendrites) segregated at later stages of crystallization. These crystals often form dendrite structures (Figure 3, right). The chemical composition of the spinel phase corresponds to magnetite/hercinite ($FeFe_2O_4$-$FeAl_2O_4$) solid solution. From the SEM data, the content of the spinel phase varies from 10-20 vol.%.

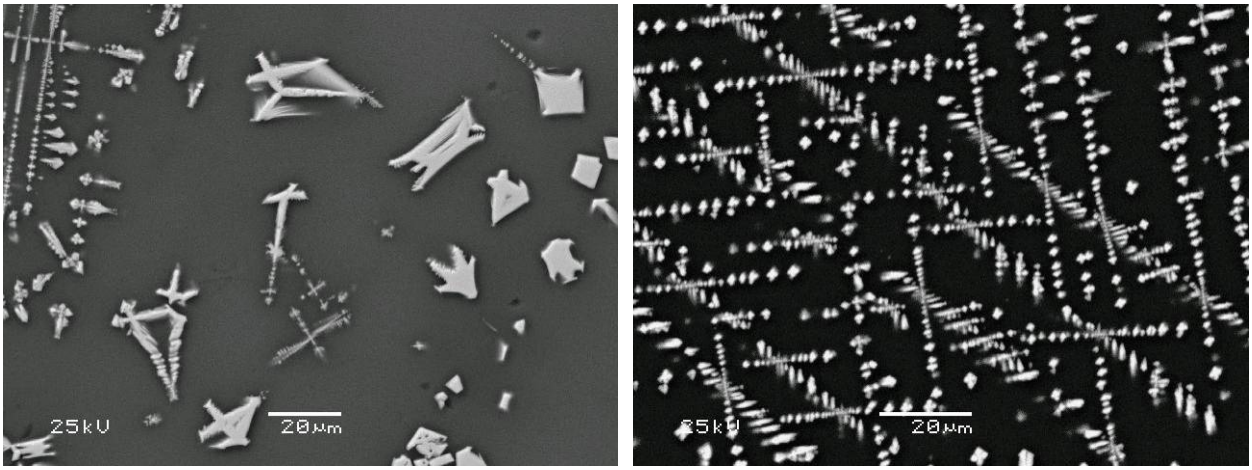

Figure 3. Primary (*a*) and secondary (*b*) spinels in glass.

On the whole as determined from optical and SEM data, the major features of all the samples are as follows:

- All the samples are composed of primarily glassy phase and minor spinel phases;
- All the samples contain gas bubbles with variable diameter (from <10 μm to >1 mm) due to incomplete refining;
- Coloring of glass varies from nearly clear to brown;
- Spinel forms both isometric grains and fine cubic crystals (~1 μm);
- Microcrystals are aggregated in bands with variable glass and spinel contents;
- Relative location of the bands is caused by flowing of various portions of the glass melt with varying viscosity;
- Wavy profile of the bands is similar to that in volcanic glasses with fluidal texture;
- No devitrification of the glass (crystallization of silicates) was found.

Major differences between the samples are as follows:

- The samples (possibly various regions of the same sample) are different in quantitative glass to spinel ratio;
- Significant differences was found in the ratio of isometric grains to cubic microcrystals;
- Fluidal texture varies; in some samples fluidity takes place only in local areas or is entirely absent;
- Degree of cracking in the thin sections varies widely. Major cracks were probably formed at preparation of the thin sections for microscopic studies.

IR spectroscopy study

IR spectra of all the samples are similar (Figure 4). IR spectra of the glasses consist of bands due to stretching (3100-3600 cm^{-1}) and bending modes (1600-1800 cm^{-1}) in the molecules of absorbed and structurally bound water, weak bands due to hydrogen bonds in the structure of glasses and numerous bands lower than 1600 cm^{-1} due to stretching and bending modes in the units forming the anionic motif of the structure of glasses.

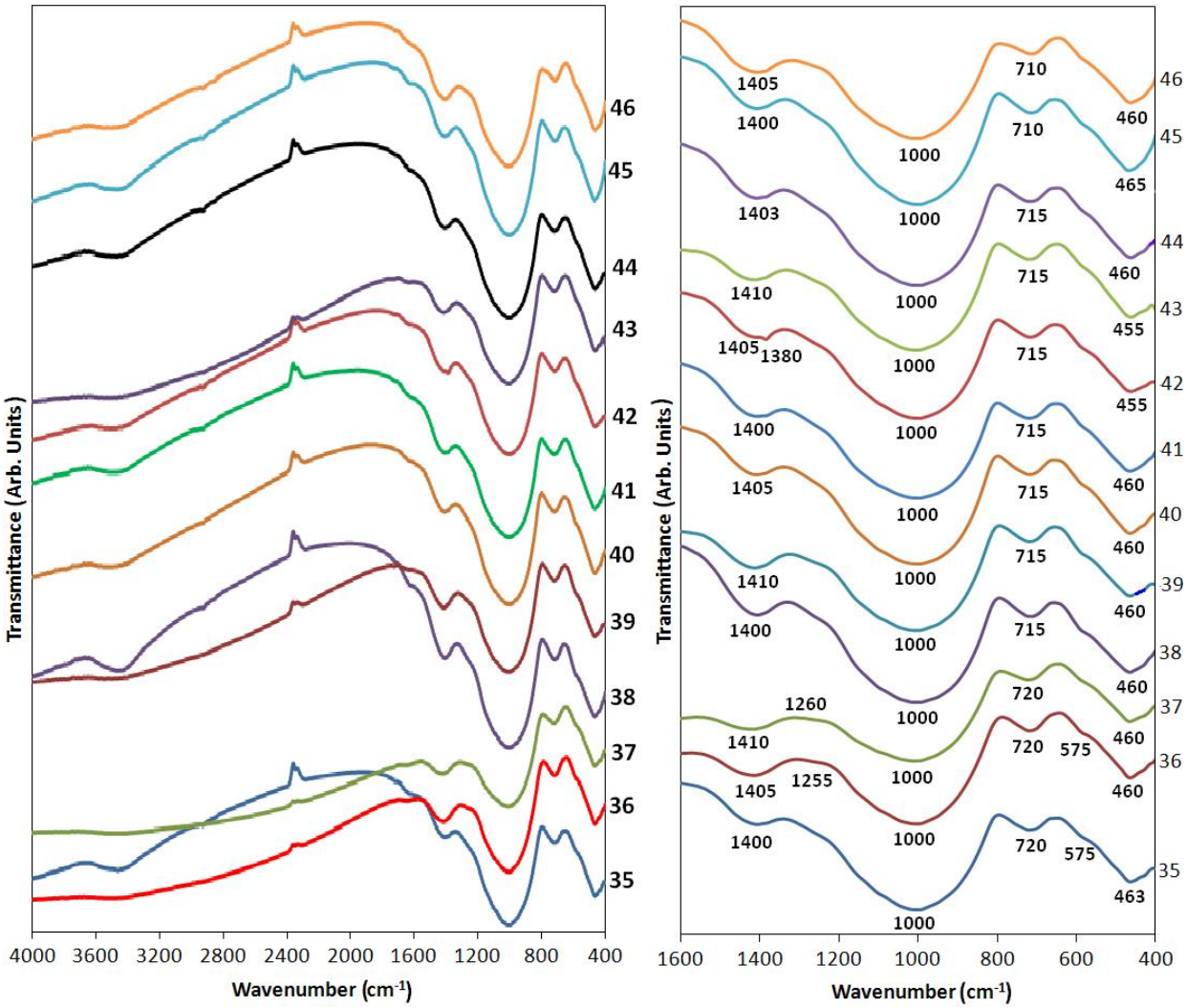

Figure 4. IR spectra of the glass samples (left) and their fragments (right).

IR spectra of all the glasses within the range of 400-1600 cm^{-1} consist of bands due to stretching and bending modes in silicon-oxygen, boron-oxygen, aluminum-oxygen and iron-oxygen structural groups. The wavenumber ranges of 1550-1300 cm^{-1} and ~1260-1270 cm^{-1} are typical of vibrations in the boron-oxygen groups with trigonally coordinated boron (boron-oxygen triangles BO_3). These bands were attributed as components of twice degenerated asymmetric valence ν_3 O−B−O vibrations (stretching

modes). The band with components ~710-730 and 650-670 cm^{-1} may be associated with twice degenerated asymmetric deformation δ (ν_4) O−B−O vibrations (bending modes) [16]. Strong absorption in both IR and Raman spectra within the range of 1150-850 cm^{-1} is caused by asymmetric ν_3 vibrations (stretching modes) in silicon-oxygen units bound to zero (850-900 cm^{-1}), one (~900-950 cm^{-1}), two (~950-1050 cm^{-1}), three (~1050-1100 cm^{-1}) and four (~1100-1150 cm^{-1}) neighboring SiO_4 tetrahedra (Q^0, Q^1, Q^2, Q^3, Q^4, respectively) [17] and, to a less extent, BO_4 tetrahedra (1000-1100 cm^{-1}) [18]. In IR spectra of all the glasses the broad band within the range of ~800-1200 cm^{-1} is multicomponent due to superposition of vibrations (stretching modes) in SiO_4 and BO_4 tetrahedra. Stretching modes of Al—O bonds in AlO_4 tetrahedra and Fe—O bonds in FeO_4 tetrahedra are positioned at 700-800 cm^{-1} and 550-650 cm^{-1}, respectively [18]. Bending modes of Si—O—Si bonds in SiO_4 tetrahedra are positioned within the range of 350-550 cm^{-1}.

As seen from Figure 4, the bands at 3300-3600 cm^{-1} and 1620-1650 cm^{-1} correlate with respect to intensity and may be attributed to stretching and bending modes in molecules of absorbed or structurally-bound water [19]. In the spectra of all the glasses, the bands due to vibrations in water molecules or Me—O—H bonds have much lower intensity than the bands due to vibration associated with the anionic motif of the glass structure

The IR spectra of all the glasses within the range of 1600-400 cm^{-1} are similar (Figure 4). This indicates that all the glasses have similar structure with respect to their anionic motif. As follows from the position of the maximum (~1000 cm^{-1}) of the strongest band 1200-800 cm^{-1}, the base of the structural network is metasilicate chains and rings where the Q^2 units are predominant.

Bridging bonds (Si—O—Fe and Si—O—Al) that bond SiO_4 and FeO_4 and AlO_4 tetrahedra and thus increasing the degree of connectedness of the glass network are positioned within the range of 950-880 cm^{-1} and may contribute to the lower wavenumber edge of the band 1200-800 cm^{-1}. The bands with a maximum at 455-463 cm^{-1} are due to bending modes in SiO_4 tetrahedra and Si—O—Si bonds (to the most extent) and Si—O—Al and Si—O—Fe bonds (to a less extent). The band with a maximum at 710-720 cm^{-1} is due to superposition of symmetric stretching modes in SiO_4 tetrahedra and asymmetric stretching modes in AlO_4 tetrahedra. The weak band observed as a shoulder at ~575 cm^{-1} is due to vibrations in FeO_4 tetrahedra. Boron in these glasses is predominantly threefold-coordinated and occurs as boron-oxygen triangles. A portion of the boron-oxygen triangles possibly enters complex borate groups linked to boron-oxygen tetrahedra.

Thus, the structural network is primarily composed of metasilicate chains and possibly rings with embedded AlO_4 and FeO_4 tetrahedra. Boron-oxygen constituents exist separately.

Raman spectroscopy study

Raman spectra of the glassy samples and their deconvolution using an Origin 9.1 software are shown in Figure 5. Spectra of samples ##39, 40, 44 and 45 differ markedly from the rest of the spectra. These glasses seem to be higher ordered or contain higher amount of crystalline phase (spinel).

All the spectra consist of the bands within the ranges of 300-600 cm^{-1}, 800-1150 cm^{-1} and weak bands at 650-800 cm^{-1} and 1200-1300 cm^{-1} and 1300-1500 cm^{-1}. Similarly to the IR spectra, these bands are due to bending and stretching modes in silicon-oxygen network, and vibrations in AlO_4, FeO_4 and BO_3 units. On the whole, Raman spectroscopic data are in a good agreement with IR spectroscopic data but computer fitting allows distinguishing of more details (Figure 5).

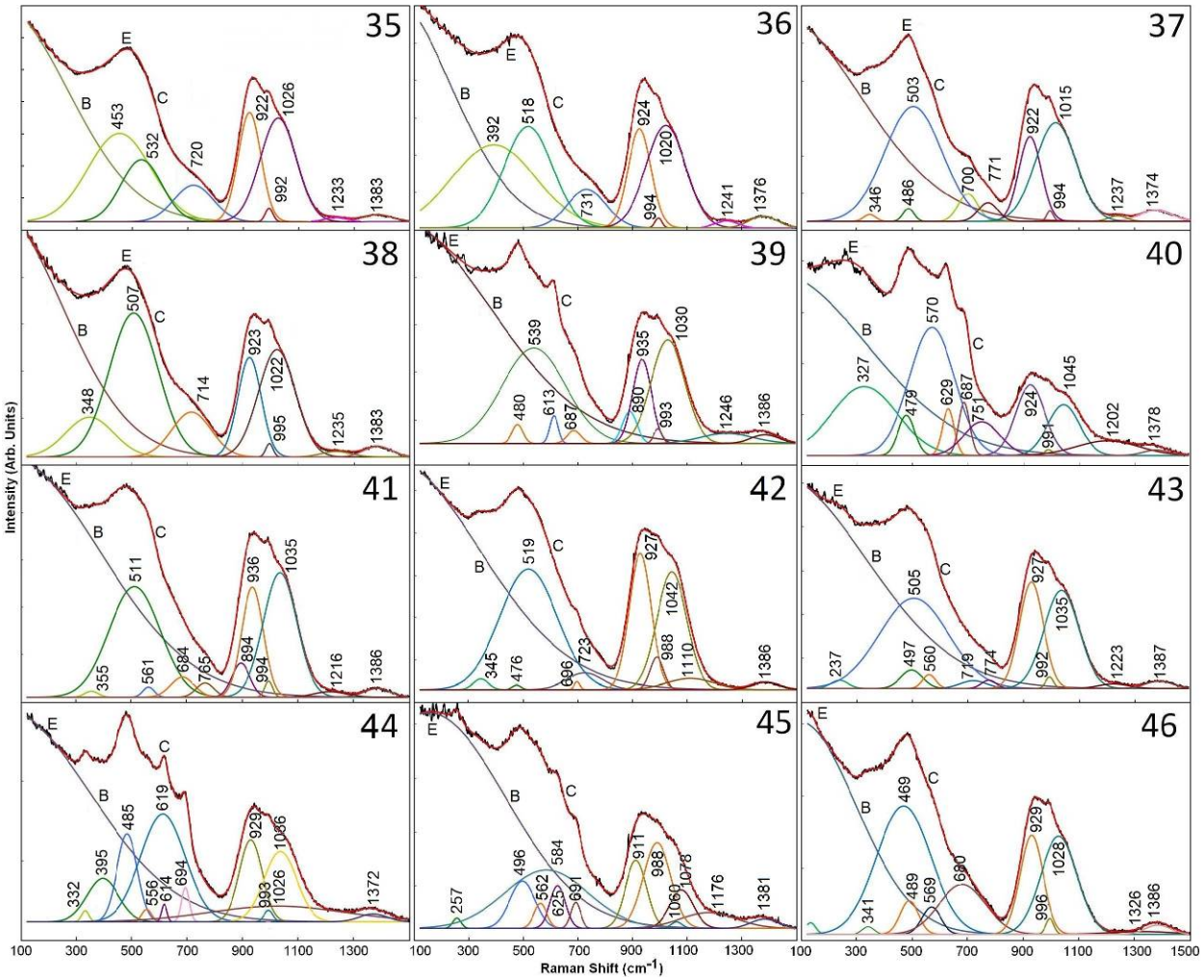

Figure 5. Raman spectra of the samples and their deconvolution.

B – baseline, C – smoothed line, E – experimental spectrum.

In the spectrum of the glassy material #35, strong bands with maxima at 453 cm^{-1}, 922 cm^{-1} and 1026 cm^{-1} are due to bending and stretching modes in SiO_4 tetrahedra and bridging bonds Si—O—Si linking SiO_4 tetrahedra. Some contribution to the band with a maximum at 922 cm^{-1} may be made by vibrations of Si—O—Al and Si—O—Fe bridging bonds. The latter are suggested to be responsible for the band with a maximum at 910 cm^{-1} observed in Raman spectra of Fe-containing silicate glasses [20]. If so, the contribution of such bonds is rather minor because of the relatively low Fe_2O_3 concentration in the glass. The band with a maximum at 532 cm^{-1} may be assigned to bending vibrations of Si—O—Si (ν_4), Si—O—Al, and Si—O—Fe bridging bonds. The band with a maximum at 720 cm^{-1} is probably due to bending modes in AlO_4 tetrahedra. Weak bands at 1383 cm^{-1} and 1233 cm^{-1} are due to vibrations in BO_3 units with various degree of polymerization. The band at 1233 cm^{-1} may also be attributed to stretching vibrations of B^{III}—O—B^{IV} bridging bonds. Since glass #35 has a value of ψ_B factor equal to approximately 2, the weak band with a maximum at 992 cm^{-1} may be assigned to stretching vibrations in BO_4 tetrahedra.

Glass #36 has higher B_2O_3 content (8.62 mol.%) and lower ψ_B value than glass #35 (Table I). Therefore, the fraction of trigonally-coordinated boron in glass #36 should be higher. It readily evident that the intensities of the bands with maxima at 1241 cm^{-1} and 1376 cm^{-1} are higher than those in the spectrum of glass #35. Overall, the spectra of both glasses are similar and differ slightly only in maxima of the bands.

The spectrum of glass #37 is more complicated. In addition to the bands observed in the spectra of samples #35 and #36 (maxima at 503 cm^{-1}, 924 cm^{-1}, 994 cm^{-1}, 1020 cm^{-1}, 1241 cm^{-1} and 1376 cm^{-1}) bands with maxima 346 cm^{-1}, 486 cm^{-1} were also found. The band at 650-800 cm^{-1} is split into two components: 700 cm^{-1} and 771 cm^{-1}. Weak bands at 346 cm^{-1}, 486 cm^{-1} and a stronger band with a maximum at 700 cm^{-1} may be attributed to vibrations in AlO_6, AlO_5 and AlO_4 polyhedra. The band with a maximum at 771 cm^{-1} is most likely due to symmetric stretching (ν_1) modes in SiO_4 tetrahedra.

The spectrum of glass #38 is similar to those of glasses #35 and #36. The difference between them is in the positions of maxima of the bands. In the spectrum of glass #38, maxima are as follows: 348 cm^{-1}, 507 cm^{-1}, 714 cm^{-1}, 923 cm^{-1}, 995 cm^{-1}, 1022 cm^{-1}, 1235 cm^{-1}, and 1383 cm^{-1}. If attribution of the bands with maxima at 507 cm^{-1}, 714 cm^{-1}, 923 cm^{-1}, 1022 cm^{-1}, 1235 cm^{-1}, and 1383 cm^{-1} is rather unambiguous, then assignment of the bands with maxima at 348 cm^{-1} and 995 cm^{-1} is indeterminate. As in the spectrum of other glasses the band with a maximum at 995 cm^{-1} may be due to stretching vibrations in BO_4 tetrahedra or Si—O—B bridging bonds. This band has low intensity that is consistent with low B_2O_3 content in glasses.

Raman spectrum of the glass #39 is markedly different from spectra of previous glasses. Along with the bands observed in spectra of other glasses (539 cm^{-1}, 935 cm^{-1}, 993 cm^{-1}, 1030 cm^{-1}, 1246 cm^{-1}, 1386 cm^{-1}) it contains weak bands with maxima at 480 cm^{-1}, 613 cm^{-1}, 687 cm^{-1}, and 890 cm^{-1}. The first three bands may be assigned to vibrations in AlO_6, AlO_5 and AlO_4 polyhedra, whereas the band with a maximum at 890 cm^{-1} – to stretching vibrations of Si—O—Al bridging bonds.

The Raman spectrum of glass #40 consists of numerous bands: strong broad bands with maxima at 327 cm^{-1}, 570 cm^{-1}, 751 cm^{-1}, 924 cm^{-1}, 1045 cm^{-1}, moderate narrow bands with maxima at 479 cm^{-1}, 629 cm^{-1}, 687 cm^{-1}, weak narrow band with a maximum at 991 cm^{-1}, and weak broad bands with maxima at 1202 cm^{-1} and 1378 cm^{-1}.

Similarly to the previous spectra the bands with maxima at 570 cm^{-1}, 751 cm^{-1}, 924 cm^{-1}, and 1045 cm^{-1} are due to bending and stretching modes in SiO_4 tetrahedra and bridging bonds Si—O—Si, Si—O—Al and Si—O—Fe; the bands with maxima at 479 cm^{-1}, 629 cm^{-1} and 687 cm^{-1} are due to vibrations in AlO_6, AlO_5 and AlO_4 polyhedra, and bands with maxima at 991 cm^{-1}, and weak bands with maxima at 991 cm^{-1}, 1202 cm^{-1} and 1378 cm^{-1} are due to vibrations in boron-oxygen constituents of the glass network.

The spectrum of glass #41 within the range of 850-1200 cm^{-1} is similar to that of glass #39. Therefore, attribution of the bands may be the same. The range lower than 850 cm^{-1} may be interpreted as superposition of the strong band due to bending vibrations in SiO_4 tetrahedra and bridging bonds Si—O—Si(Al, Fe) and weak bands due to vibrations in MeO_x polyhedra.

The spectrum of glasses #42, #43 and #46, similarly to the spectra of other glasses in the same group, may be deconvoluted into the bands due to stretching and bending vibrations in silica-oxygen, aluminum-oxygen, iron-oxygen, and boron-oxygen polyhedra.

A set of bands obtained by deconvolution of the spectra of glasses #39, #40, #44, and #45 within the range of 850-1200 cm^{-1} into components is similar to those obtained from the spectra of different glasses. The difference is within the range of 300-850 cm^{-1} where numerous bands are required to achieve good alignment between experimental and fitted spectra.

Overall, for the spectra of all the glasses within the range of 850-1200 cm^{-1} the best fit is achieved by suggestion of overlapping of three major components with maxima at 911-936 cm^{-1}, 988-996 cm^{-1} and 1020-1045 cm^{-1}. For the best fit for spectra of glasses #39 and #41, an additional line with a maximum at 890-894 is required. So, it can be concluded that the structure of glasses is composed of metasilicate chains and rings containing incorporated AlO_4 and FeO_4 as well as minor BO_4 tetrahedra. Major BO_4 tetrahedra and BO_3 triangles form complex borate units and are present as separate constituents.

Computer fitting within the range of 300-850 cm^{-1} is much more complicated. This range consists of numerous bands due to bending vibrations in silicon-oxygen networks with incorporated MeO_4 tetrahedra, symmetric stretching vibrations in silicon-oxygen networks and stretching vibrations of Me—O bonds in MeO_n polyhedra as well as the bands due to stretching and bending vibrations of Me—O bonds in spinel crystals [18]. This makes attribution of the bands in this range rather difficult and ambiguous.

Nevertheless some general suggestions concerning attribution of the bands within this range may be performed. If to compare Raman spectra of glasses #45 and #46 related to two different groups, then we can see some similarity in behavior of the bands: i) occurrence of a strong broad band due to bending vibrations of the bonds in silica-oxygen network and bridging bands Si—O—Me bonding SiO_4 and MeO_4 tetrahedra; ii) occurrence of the bands with maxima at 496 cm^{-1} or 489 cm^{-1} and 562 cm^{-1} or 569 cm^{-1} (for glasses #45 and #46, respectively). At the same time the spectrum of glass #46 contains a broad band centered at 680 cm^{-1} whereas in the spectrum of glass #45 a weak narrow band centered at 691 cm^{-1} is present. Moreover, the spectrum of glass #45 contains an additional narrow band centered at 625 cm^{-1}. If broad bands are due mainly to vibrations in low-symmetry structural units in a random glass network, then narrow band are due probably to vibrations in high-symmetry structural units of the spinel structure phase.

The chemical composition of spinel phase may be represented by the general formula $(Mg,Mn,Ni,Cu)^{2+}(Fe,Al)^{3+}O_4$. Taking into account low MgO, NiO and CuO concentrations, major contribution to these bands is due to vibrations of Fe—O and Al—O bonds in FeO_4 and AlO_4 tetrahedra, and to a much less extent, Mn—O and Fe—O bonds in MnO_6 and FeO_6 octahedra. Thus, the bands within the range of 300-500 cm^{-1} may be associated with vibrations of Mn—O and Fe—O bonds in MnO_6 and FeO_6 octahedra in the spinel structure. The bands at 550-650 are due mainly to vibrations of Fe—O bonds in FeO_4 tetrahedra in both spinel and glass structures and, to some extent in FeO_6 octahedra. Vibrations of Al—O bonds in AlO_4 tetrahedra in both spinel and glassy phases are positioned at 650-750 cm^{-1}. For more precise simulation of the spectra within the range of 300-850 cm^{-1} special study with the use of model compounds (surrogates) with the known structures is required.

CONCLUSIONS

All the glasses studied are composed of predominantly vitreous phase and minor spinel structure phase. Spinel forms both isometric grains and cubic microcrystals (~1 μm). Microcrystals are aggregated in bands with variable glass and spinel contents. IR and Raman spectroscopic study revealed that the structure of all the glasses are similar and are composed of metasilicate chains and rings containing incorporated AlO_4 and FeO_4 as well as minor BO_4 tetrahedra. FeO_6 octahedral units may also be present. In the structure of all the glasses, trigonally-coordinated boron dominates over tetrahedrally-coordinated boron. With that said, major BO_4 tetrahedra and BO_3 triangles form complex borate units and are present as separate constituents

REFERENCES

1. R.C.P. HILL, J.G. REYNOLDS, and P.L. RUTLAND, "Comparing Hanford and Savannah River Tank Wastes," *Radwaste Solutions*, [1] 32 (2012).
2. K.M. FOX, D.H. MILLER, and T.B. EDWARDS, *Preliminary Frit Development and Melt Rate Testing for Sludge Batch 6 (SB6)*, SRNL-STI-2009-00440, 2009.
3. A.A. APPEN, *Chemistry of Glass* (Russ.), Khimiya, Leningrad, USSR (1974).
4. A.F. WELLS, *Structural Inorganic Chemistry*, Fifth Edition, Oxford University Press, Oxford, England (1986).
5. R.D. SHANNON. "Revised effective Ionic Radii and Systematic Studies of Interatomic Distances in Halides and Chalcogenides," *Acta Cryst*. **A 32**, 751 (1976).
6. M.E. MILBERG, J.G. O'KEEFE, R.A. VERHELST, and H.O. HOOPER. "Boron Coordination in Sodium Borosilicate Glasses," *Phys. Chem. Glasses*. **13** [3], 79 (1972).
7. Y.n. YUN and P.J. BRAY. "Nuclear Magnetic Resonance Studies in the Glasses in the System Na_2O-B_2O_3-SiO_2," *J. Non-Cryst. Solids*. **27**, 363 (1978).
8. W.J. DELL, P.J. BRAY, and S.Z. XIAO. "^{11}B NMR Studies and Structural Modelling of Na_2O-B_2O_3-SiO_2 Glasses of High Soda Content," *J. Non-Cryst. Solids*. **58**, 1 (1983).
9. R. MARTENS and W. MÜLLER-WARMUTH. "Structural Groups and their Mixing in Borosilicate Glasses of Various Compositions – an NMR Study," *J. Non-Cryst. Solids*. **265**, 167 (2000).
10. A. DUDDBRIDGE, M.M. ISLAM, D. HOLLAND, and C.R. SCALES. Chemical Durability Studies of Waste-Simulant Doped Borosilicate Glasses," *Mater. Res. Soc. Symp. Proc*. **807**, 145 (2004)
11. D. HOLLAND, B.G. PARKINSON, M.M. ISLAM, A. DUDDBRIDGE, J.M. RODERICK, A.P. HOWES, and C.R. SCALES. "NMR Investigation of Cation Distrubution in HLW Wasteform Glass," *Mater. Res. Soc. Symp. Proc.* **1107**, 199 (2008).
12. H. DETERS, A. S. S. de CAMARGO, C. N. SANTOS, C. R. FERRARI, A. C. HERNANDES, A. IBANEZ, M. T. RINKE, and H. ECKERT, "Structural Characterization of Rare-Earth Doped Yttrium Aluminoborate Laser Glasses Using Solid State NMR." *J. Phys. Chem*. C **113**, 16216 (2009).
13. B.G. PARKINSON, D. HOLLAND, M.E. SMITH, C. LARSON, J. DOERR, M. AFFATIGATO, S.A. FELLER, A.P. HOWES, and C.R. SCALES, "Quantitative Measurement of Q^3 Species in Silicate and Borosilicate Glasses using Raman Spectroscopy," *J. Non-Cryst. Solids*. **354**, 1936 (2008).
14. C.M. JANTZEN, and K.G. BROWN."Predicting the Spinel–Nepheline Liquidus for Application to Nuclear Waste Glass Processing. Part I: Primary Phase Analysis, Liquidus Measurement, and Quasicrystalline Approach," *J. Amer. Ceram. Soc*. **90** [6] 1866 (2007).
15. S.V. STEFANOVSKY, J.C. MARRA. "The Effect of Waste Loading and Glass Structural Factors on Structure and Chemical Durability of SB2 and SB4 SRS Waste Glasses," Proceedings of the Waste Management 2011 Conference., Phoenix, AZ, February 27- March 3, 2011. Paper 11397 (2011).
16. V.A. KOLESOVA, "Vibrational Spectra of Alkali-Borate Glasses," *Glass Phys. Chem.* (Russ.) **12**, 4 (1986).
17. V.N. ANFILOGOV, V.N. BYKOV, and A.A. OSIPOV. *Silicate Melts* (Russ.), Nauka, Moscow, Russia, 2005.
18. I.I. PLYUSNINA. *Infrared Spectra of Minerals* (Russ.), MSU Publishers, Moscow, Russia (1977).
19. K. NAKAMOTO. *Infrared Spectra of Inorganic and Coordination Compounds*, John Wiley & Sons, Inc. New York – London (2009).

20. V. MAGNIEN, D.R. NEUVILLE, L. CORMIER, J. ROUX, J-L. HAZEMANN, O. PINET, and P. RICHET "Kinetics of Iron Redox Reactions in Silicate Liquids: a High-Temperature X-ray Absorption and Raman Spectroscopy Study," *J. Nucl. Mater*. **352**, 190 (2006).

ACKNOWLEDGEMENTS

The work was performed under financial support from Savannah River National Laboratory (subcontract No. AC69549N). Authors thank Dr. A.A. Akatov (Institute of Technology, St-Petersburg) for record of IR spectra and Dr. A.A. Shiryaev (Frumkin Institute of Physical Chemistry and Electrochemistry RAS) for record of Raman spectra. Special thanks to Dr. B.I. Omelyanenko for his help in optical microscopy study of glasses and Dr. Y.G. Teplyakov for his contribution in the study on deconvolution of Raman spectra.